Soft Matter

PAPER

View Article Online
View Journal | View Issue

Cite this: *Soft Matter*, 2023, **19**, 1212

Effects of the polymer glass transition on the stability of nanoparticle dispersions†

Douglas M. Scott, [a] Robert K. Prud'homme [a] and Rodney D. Priestley *[ab]

Received 4th December 2022,
Accepted 13th January 2023

DOI: 10.1039/d2sm01595a

rsc.li/soft-matter-journal

In addition to the repulsive and attractive interaction forces described by Derjaguin–Landau–Verwey–Overbeek (DLVO) theory, many charged colloid systems are stabilized by non-DLVO contributions stemming from specific material attributes. Here, we investigate non-DLVO contributions to the stability of polymer colloids stemming from the intra-particle glass transition temperature (T_g). Flash nanoprecipitation is used to fabricate nanoparticles (NPs) from a library of polymers and dispersion stability is studied in the presence of both hydrophilic and hydrophobic salts. When adding KCl, stability undergoes a discontinuous decrease as T_g increases above room temperature, indicating greater stability of rubbery NPs over glassy NPs. Glassy NPs are also found to interact strongly with hydrophobic phosphonium cations (PR_4^+), yielding charge inversion and intermediate aggregation while rubbery NPs resist ion adsorption. Differences in the lifetime of ionic structuration within mobile surface layers is presented as a potential mechanism underlying the observed phenomenon.

Introduction

Polymeric nanoparticle (NP) dispersions have shown promise for use in applications ranging from the encapsulation and delivery of active ingredients,[1,2] support of catalysts as carrier matrices,[3,4] formation of highly stable Pickering emulsions,[5,6] to the growth of colloidal crystals.[7] While the advantageous properties of polymeric NP dispersions stem from their high specific surface area, versatile chemistries, and morphologies, maintaining these properties requires the suppression of aggregation and flocculation, which arise from attractive van der Waals and hydrophobic interactions between independent diffusing particles.[8] As a result, NP dispersions are commonly formulated with stabilizers that impart a repulsive steric and/or electrostatic interaction between particles.[9,10] Steric repulsion provides stability *via* the unfavorable overlap of solvated layers on the NP surfaces. In contrast, electrostatic repulsion relies on the overlap of electric double layers (EDLs) arising from the presence of ionized sites on the particle surface. In the case of electrostatic repulsion, the addition of salt enables the tuning of this contribution by compressing the EDL, enabling attractive interactions to dominate at small particle-particle separations, *i.e.*, the so-called salting out effect. The sum of both attractive and repulsive interactions is given by classic DLVO (Derjaguin–Landau–Verwey–Overbeek) theory, which provides a useful framework for discussing the stability of NP dispersions.[8]

In addition to repulsive steric and electrostatic forces and attractive van der Waals forces, a class of non-DLVO interactions resulting from differences in hydration, surface roughness, and chemical heterogeneities has been characterized for many interacting systems. These non-DLVO interactions are commonly invoked to explain anomalous interaction forces at close separations as well as in complex mixtures.[11–15] In systems where the observed interactions cannot be attributed to known non-DLVO contributions, additional short-range contributions must be empirically fit to stability and atomic force measurements.[16,17] Given the diversity of systems studied, and the high variability in measurement approaches, connecting measured interaction forces and dispersion stabilities to underlying physical mechanisms is an ongoing effort within the field.

Electrostatic-stabilized polymer NPs represent a valuable class of colloids given their tunable interactions, chemistries, and morphologies. While the size stability of these dispersions can be correlated with formulation parameters such as particle size, salt concentration, and surface charge group density,[18–21] the effect of the underlying polymer mobility, characterized by the glass transition temperature (T_g), has not been thoroughly studied.[22,23] When preparing polymer NPs *via* precipitation, the T_g has been shown to define vitrification timescales, allowing

[a] *Department of Chemical and Biological Engineering, Princeton University, Princeton, NJ 08544, USA*
[b] *Princeton Institute for the Science and Technology of Materials, Princeton University, Princeton, NJ 08544, USA. E-mail: rpriestl@princeton.edu; Fax: +609-258-5599; Tel: +609-258-5721*

† Electronic supplementary information (ESI) available: Descriptions of the methods and materials used in this study as well as a summary of the diameters and zeta potentials of polymeric NPs produced *via* FNP. Aggregation trends for NP dispersions salted with KCl as well as PS and PI NP dispersions with NH_4F and GdmCl. See DOI: https://doi.org/10.1039/d2sm01595a

for complex morphologies to form from the kinetic arrest of phase separation in polymer blend NPs.[24,25] In addition, there is now substantial evidence that there exists a surface layer with a T_g suppressed compared to the bulk value for hydrophobic polymer NPs dispersed in water.[26,27] The thickness of the mobile surface layer is estimated to be between ~3–7 nm. Therefore, as particle size is reduced, and the surface area to volume ratio increases according to $\sim 1/r$, the influence of the mobile surface layer on overall NP dynamics grows, eventually leading to a decrease in NP T_g.[26,28,29] Hence, although the impact of T_g on particle morphology and surface dynamics has been studied, its effect on colloidal stability as a source of non-DLVO contributions has yet to be systematically evaluated beyond early studies focused on the annealing of glassy latex particles possessing vitrified surface layers of charged initiator end groups.[22,23] In this work, we investigate the effects of polymer T_g on colloidal stability in the presence of both hydrophilic and hydrophobic salts through the study of polymeric NP dispersions fabricated from a broad library of polymers.

Experimental methods

Materials

Eleven hydrophobic polymers with midpoint T_g's ranging from −104 to 158 °C were chosen to prepare NPs (listed in ascending T_g): poly(1,4-butadiene) (PB), poly(*cis*-isoprene) (PI), poly(*n*-nonyl methacrylate) (PnNonMA), poly(*n*-hexyl methacrylate) (PnHexMA), poly(*n*-butyl methacrylate) (PnBuMA), poly(*n*-propyl methacrylate) (PnPrMA), poly(*iso*-butyl methacrylate) (PiBuMA), polystyrene (PS), poly(*t*-butyl methacrylate) (PtBuMA), poly(4-bromostyrene) (PBrS), and poly(4-vinyl phenol) (P4HS) (chemical structures, T_g's, molecular weights, and sourcing information are provided in the ESI†). As all experiments were conducted at room temperature (RT ~ 25 °C), resultant polymer NPs were classified as 'glassy' for those with $T_g >$ RT and 'rubbery' for those with $T_g <$ RT.

Nanoparticle preparation

Flash nanoprecipitation (FNP), a rapid and scalable colloid fabrication platform, was used to produce NPs of these polymers.[30,31] First, polymers were dissolved in tetrahydrofuran (THF, HPLC Grade, Fisher Scientific) at 5 mg mL^{-1} under gentle stirring for 3 h. Using a confined impingement jet (CIJ) mixer, 0.5 mL of a polymer solution was impinged against 0.5 mL of DI H_2O (filtered *via* Milli-Q IQ 7000 Ultrapure system) and the effluent was flown into a stirred 4 mL reservoir of H_2O to yield an overall 10-fold dilution of the original inlet solution.[32]

Following FNP, dispersions were subjected to rotary evaporation (Büchi Rotavapor R-300) to remove the 10 vol% THF fraction remaining in the aqueous phase. As H_2O may have also been removed during evaporation, and to avoid discrepancies between precipitation efficiencies among polymers, thermal gravimetric analysis (TA Q50) was used to measure final NP dispersion concentrations in which 100 μL of a NP dispersion was carefully pipetted onto a tared platinum pan and heated to 100 °C for 15 min, followed by 120 °C for 30 min to ensure complete drying. From the remaining sample mass measured, the mass concentration of the NP dispersion was calculated and used for subsequent experiments. Lastly, particle size and zeta potential were measured using dynamic light scattering (DLS) and continuously-monitored phase-analysis light scattering (cmPALS), respectively (Anton Paar Litesizer 500).

Salting experiments

The addition of potassium chloride (KCl), tetrabutylphosphonium bromide (TBPB), tetraphenylphosphonium bromide (TPPB), guanidium chloride (GdmCl), or ammonium fluoride (NH_4F) to NP dispersions was conducted in a manner to minimize mixing time and reduce spatial heterogeneity of salt concentrations which could lead to premature aggregation. Samples of NP stock dispersions were first diluted with appropriate volumes of H_2O in 1.5 mL centrifuge tubes. Holding the tubes over a vortex mixer (Fisherbrand), appropriate volumes of salt stock solutions were quickly injected into the samples, which were immediately capped and vortexed for 5 seconds at 3000 rpm. In experiments with logarithmic salting series (TBPB and TPPB), stock solutions were created with 10^2 order of magnitude spacing to minimize volumetric pipetting error across samples. Salted dispersions were then allowed to sit for 24 hours at RT after which particle size and zeta potential were measured.

Results and discussion

Nanoparticles of all eleven polymers were produced by FNP, a versatile precipitation process in which fast micromixing between polymer solutions and antisolvents produce significant supersaturation and rapid chain collapse.[18,33] Following the diffusion-limited aggregation of the collapsed polymer nuclei, particles were found to be stabilized by a negative surface potential which has been attributed to the hydrophobic adsorption of naturally-occurring anions from the surrounding aqueous medium.[34,35] NP size and zeta potential for all polymers NP dispersions were measured and are presented in Fig. S2 and S3 within the ESI.†

Stability trends in the presence of a hydrophilic salt

In colloidal dispersions, the addition of a hydrophilic salt such as KCl results in the compression of the EDL surrounding the NPs, screening of the electrostatic repulsion arising from their overlap at close proximity, and an eventual loss of stability as attractive interactions dominate. The threshold salt concentration for this instability, termed the critical coagulation concentration (CCC), sets the upper limit for salt addition in dispersions beyond which particle begin to aggregate. This is important in applications such as Pickering emulsions wherein charged NPs encounter repulsion from charged oil/water interfaces, requiring the addition of salt to screen this electrostatic repulsion and enable interfacial adsorption while remaining below the CCC.[21] To assess stability for polymer NPs spanning

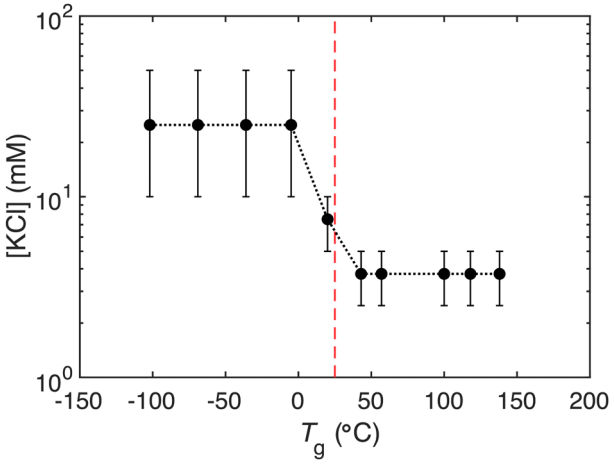

Fig. 1 Effect of polymer T_g on the stability of NP dispersions in the presence of KCl. The ordinate threshold [KCl] is defined by the concentration at which a 25% increase in particle diameter over 24 hour was observed. Room temperature (25 °C) is indicated on the plot *via* a dashed red line. Error bars represent the next nearest measured values of [KCl] between which the instability threshold is observed.

the range of T_g's, KCl was added at concentrations ranging from 0.5–50 mM to each NP dispersion ([NP] = 0.1 mg mL^{-1}), and particle size was measured after 24 hours (see Fig. S5, ESI†). Glassy NPs were found to aggregate for [KCl] > 2.5 mM with sharp increases in aggregate size. In contrast, rubbery NPs showed instability for [KCl] > 10 mM followed by gradual increases in size from reformation into denser aggregates due to higher chain mobility.[19] Defining a threshold [KCl] in which particle sizes increased by 25%, Fig. 1 shows a sharp decline in NP stability as polymer T_g exceeds RT, indicating greater stability for rubbery NPs compared to glassy ones. Interestingly, for the case of poly(*n*-butyl methacrylate) (PnBuMA) for which T_g (~20 °C) lies within proximity of RT, this threshold is found to lie at an intermediate value of [KCl] = 7.5 mM.

Given the distinct differences in salt stability between glassy and rubbery NPs across multiple chemistries, the connection between T_g and stability was further investigated *via* kinetic studies of poly(*n*-propyl methacrylate) (PnPrMA) NP aggregation at temperatures above and below T_g. PnPrMA was selected as a glassy polymer with an intermediate T_g (~43 °C) adequately above RT but sufficiently below 100 °C to minimize evaporation during tests. To perform the kinetic studies, PnPrMA NP dispersions and KCl solutions were independently heated in an oven at 60 °C. At the same time, the DLS sample holder was equilibrated to target incubation temperatures of 25, 35, 40, 45, or 55 °C, respectively. As shown in Fig. 2a, the procedure of starting from the rubbery state at high temperature and cooling to a lower target temperature was chosen to avoid potential aggregation. In the converse approach, initially glassy dispersions would have become unstable as they were slowly heated above T_g in the DLS sample holder. This experimental design was informed by the observed trend in Fig. 1 which is represented as the dashed boundary within Fig. 2a separating stable and unstable regions. For each test, the pre-heated KCl solution was quickly mixed with the PnPrMA NP dispersion to yield a 0.1 mg mL^{-1} NP and a 10 mM KCl mixture. 10 mM was chosen for [KCl] as it was sufficiently above the previously measured glassy stability threshold of ~3.75 mM at RT. The mixture was then immediately transferred to the DLS sample holder upon which a timed-series measurement was initiated. Within the sample holder, the salted dispersion cooled to the target temperature and particle aggregation was continuously measured.

Fig. 2b shows particle size over time for the five incubation temperatures. As the temperature increased from RT but remained below the NP T_g, the onset time of aggregation was found to decrease, agreeing with classical DLVO theory in which the electrostatic energetic barrier to aggregation (W), depressed from salt screening, was overcome with higher

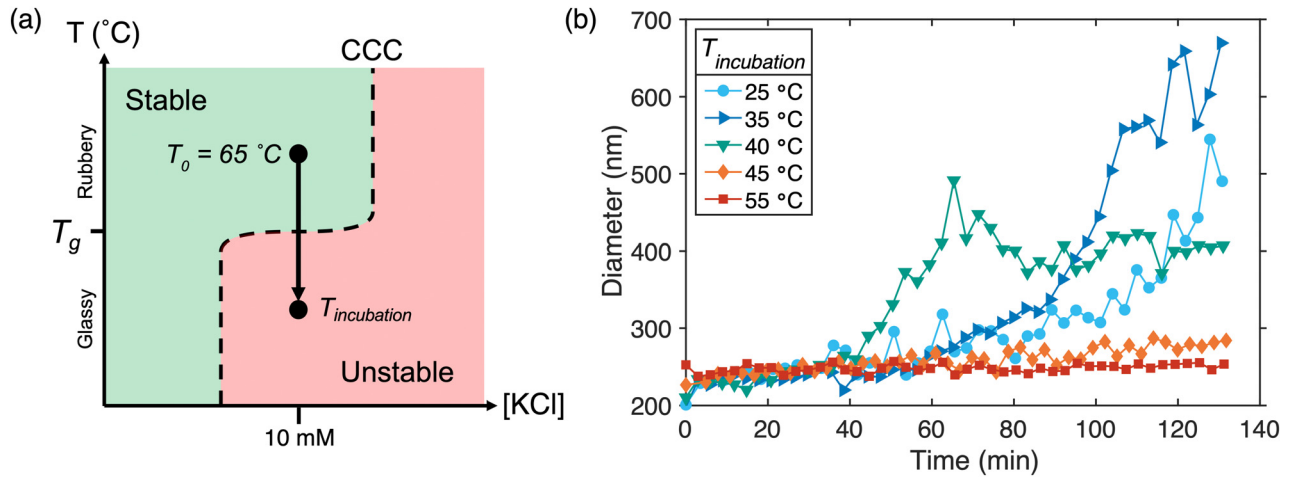

Fig. 2 The effect of temperature on the stability of PnPrMA NPs: (a) Schematic of the experimental set-up informed by the underlying phase diagram from Fig. 1 in which salted NP dispersions initially at T_0 = 65 °C are cooled to a target $T_{incubation}$ and NP size is continuously monitored. (b) Trajectories of NP diameter over time for increasing $T_{incubation}$. For $T_{incubation} < T_g$ wherein PnPrMA NPs are glassy (25, 35, 40 °C), aggregation is observed. In contrast, for $T_{incubation} > T_g$, aggregation was not observed within the experimental timeframe.

frequency as thermal energy (k_bT) increased. However, as the temperature exceeded the NP T_g (45, 55 °C) and the NP became rubbery, no aggregation was observed; hence, a reversal from the prior trend. This discontinuity in aggregation behavior for NPs formulated from a single polymer further supports the effect of the glassy state of polymers on NP stability in which rubbery NPs demonstrated enhanced stability in comparison to glassy particles. Whether independently varying T_g *via* differences in monomer chemistry or adjusting dispersion temperature (T), the relation between NP stability behavior and the glassy state of NPs is shown to be consistent.

Stability trends in the presence of hydrophobic salts

Having already seen that T_g plays an important role in polymer NPs formulated with hydrophilic salts that interact with the EDL surrounding NPs, we explored if T_g also played an important role in the stability of NPs formulated with hydrophobic salts which interact with the polymer NP itself. Specifically, hydrophobic salts can adsorb to particle surfaces *via* hydrophobic interactions, manifesting as potential-determining ions. Symmetric hydrophobic ions such as substituted ammonium, phosphonium, and borate derivatives have been shown to strongly modify electrophoretic mobilities of PS latexes beginning at extremely low concentrations (10^{-6} M).[16,17,36–38] Symmetric hydrophobic cations have also been demonstrated as effective charge modifiers to controllably screen the zeta potential of silica NPs,[39–41] enabling their use as Pickering emulsifiers.[42] To further investigate whether T_g impacts interactions and stability in the presence of hydrophobic ions, two symmetric phosphonium salts, tetrabutylphosphonium bromide (TBPB) and tetraphenylphosphonium bromide (TPPB) were added to the polymeric NP dispersions.

To investigate the effect of T_g on stability in the presence of hydrophobic ions, PS and PI were selected as candidate glassy and rubbery polymers, owing to their similar interfacial tensions with water and well-characterized phase separation in polymer NPs which enable the formation of tunable complex morphologies including Janus, core–shell, and multi-lobed NPs.[4,24,25,43] Hydrophobic phosphonium salts were added to PS and PI NP dispersions at concentrations spanning multiple decades (10^{-4}–10^{2} mM). For PS NPs, the addition of phosphonium salts resulted in concentration regimes in which dispersions were unstable, forming macroscopic aggregates due to fast rates of aggregation, followed by re-entrant stability at higher concentrations. Conversely, PI NPs only exhibited a singular instability threshold near [TBPB] = 10^{-1} mM (Fig. 3a) above which turbid dispersion were formed. In the case of TPPB (Fig. 3b), both the intermediate regime of instability (PS) and instability threshold (PI) shifted to lower concentrations than observed for TBPB, indicative of enhanced hydrophobic adsorption stemming from the greater hydrophobicity provided by the phenyl groups.

To understand the mechanism underlying the distinct size trends for PS and PI NPs, zeta potential (ζ) was measured for each hydrophobic salt concentration (Fig. 3c). For PS NPs, ζ exhibited a large increase with logarithmic increases in [TBPB] and [TPPB], undergoing charge inversion at lower concentrations, well below the regime where charge screening effects dominate ($\sim 10^{1}$ mM), indicating the strong adsorption of hydrophobic cations onto the glassy NP surface to become potential-determining ions. Consequently, the salt concentration regimes in which ζ inversion ($|\zeta| < 25$ mV) and positive ζ (>25 mV) were measured respectively corresponded to the observed regimes of PS NP aggregation and re-entrant stability. The greater hydrophobicity of TPPB enhanced its adsorption to the PS NP surface, shifting the onset of increases in ζ and aggregation to lower concentrations (10^{-4} mM). Conversely, the ζ of PI NPs exhibited minimal variation for concentrations below 10^{-2} mM, followed by partial inversion for both phosphonium derivatives. As a result, PI NPs showed a singular instability threshold concentration for both salts with no re-entrant stability.

To see whether the distinct trends between ζ and hydrophobic salt concentration observed for PS and PI NPs could be generalized across a range of polymer T_g's, ζ was measured for TBPB-salted NP dispersions formulated from ten polymers with T_g's spanning −104–158 °C (Fig. 4). As [TBPB] increases, the ζ of all polymers NPs increased while variance among polymers

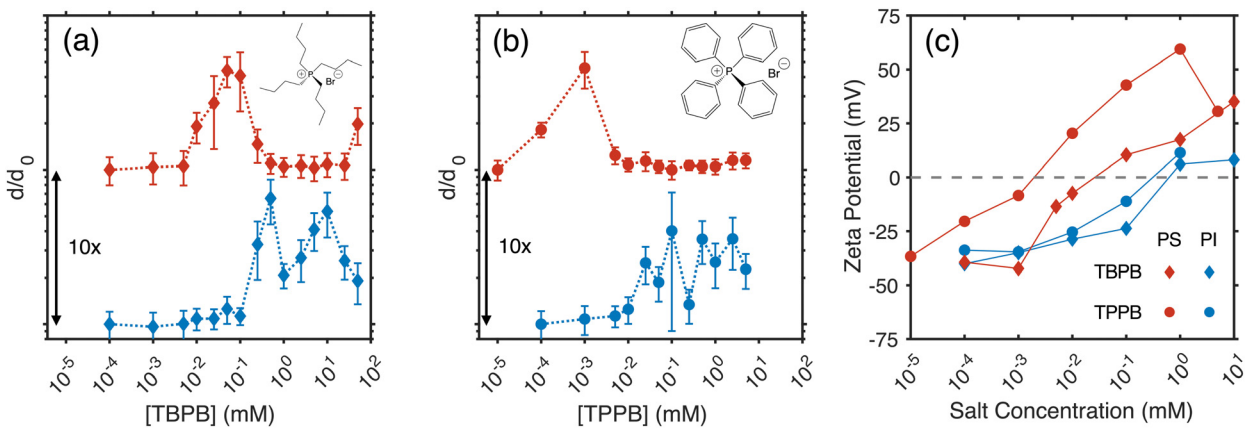

Fig. 3 (a and b) Size stability trends for PS and PI NPs in the presence of (a) TBPB and (b) TPPB and (c) the corresponding inversion of zeta potentials. [NP] = 0.1 mg mL^{-1}.

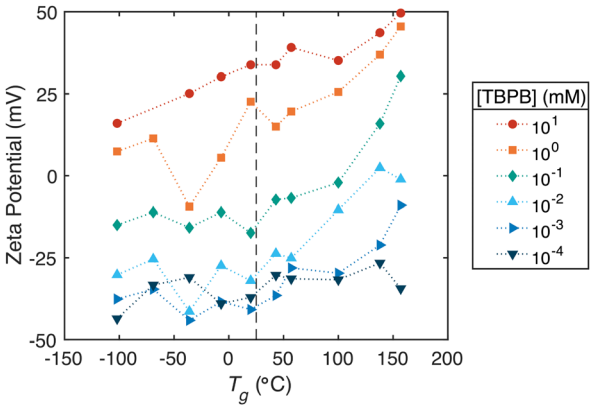

Fig. 4 The effect of T_g on the average zeta potential of polymeric NPs with logarithmic increases in [TBPB]. RT (25 °C) is indicated on the plot by a vertical dashed line.

exhibited distinct trends: (1) for [TBPB] = 10^{-4}–10^{-1} mM, the ζ of rubbery NPs showed little variation while glassy NPs, especially those with high T_g (>100 °C), showed a positive correlation between ζ and T_g; (2) for [TBPB] = 10^0 mM, glassy NPs maintained the positive correlation while rubbery NPs exhibited scatter in ζ across T_g's, potentially attributable to the high sensitivity of ζ to slight differences in net surface charge density, σ, near charge inversion as indicated by the Grahame equation ($\zeta \sim \sinh^{-1} \sigma$); (3) for [TBPB] = 10^1 mM, a positive correlation between ζ and T_g emerged, spanning the entire range of T_g's tested.

Consistent with the trend previously observed for PI NPs, rubbery NPs exhibited a 'induction' [TBPB] range ([TBPB] $\leq$ 10^{-1} mM) wherein negligible charge inversion was measured. This in turn differentiated the initial trajectories of charge inversion between rubbery and glassy NPs. At high [TBPB] where charge inversion was observed for all polymer NPs, ζ was found to continuously increase with T_g across both sets of rubbery and glassy NPs, suggesting differences in polymer mobility, characterized by the difference between T and T_g, may directly affect the equilibrium adsorption of hydrophobic ions onto NP surfaces. This behavior lies in contrast to the discontinuity in CCC measured between rubbery and glassy NPs when screening electrostatic repulsion with a hydrophilic salt such as KCl.

Proposed mechanisms connecting stability and T_g

While the mechanism underlying the observed connection between polymer NP stability in salted dispersions and T_g is not fully understood, these results may suggest an adsorption-mediated mechanism such as surface structuration[44,45] or charge-regulation.[46]

Surface structuration was demonstrated by Siretanu *et al.* for glassy polymer thin films submerged in degassed salt solutions where ion adsorption and resultant interfacial charge interactions were found to amplify surface fluctuations, thereby deforming the film surface.[44,45] Specifically, degassed solutions were required to eliminate the presence of nanobubbles which were posited to accumulate on hydrophobic surface and interfere with ion adsorption through occupation of the interfacial region of reduced water density wherein hydrophobic ions would preferentially localize.[36] The extent of these surface deformations has been directly linked to surface plasticization *via* repulsive confinement effects which reduce the local T_g at the film-aqueous phase interface.[47] For nanoparticles with diameters on the order of the reported characteristic size of nanobubbles observed by AFM (50–100 nm),[48] their high curvature would make the accumulation of nanobubbles on their surfaces highly unlikely. As a result, the adsorption of cations onto the surface of glassy NPs in aqueous media at ambient conditions may lead to deformation and structuration of the particle surface. Further, significant structuration was observed for hydrophobic ionic species similar to TPPB (*e.g.* Ph_4AsCl, Ph_4BNa),[44] suggesting an interplay between structuration and the observed charge inversion of NPs in this study. If the deformation of interfacial polymer layers at NP surfaces enables adsorbed ions to adopt lower energy configurations, the lifetime of these deformations, defined by the polymer mobility given by the proximity of T_g to RT, may manifest in differences between glassy and rubbery NPs. For glassy polymer NPs with partially-mobilized interfacial layers, these deformations persist on long timescales, enhancing the adsorption of hydrophobic ions while deformations of the highly mobile surface of rubbery NPs would persist on shorter timescales, frustrating the ability of adsorbed ions to adopt favorable configurations on a fluctuating surface, thereby diminishing adsorption. We readily admit that this proposed mechanism is speculative. The phenomena certainly invites further studies to elucidate the fundamental mechanisms responsible for the experimental results.

While the effect of ion adsorption on NP stability is prominent for hydrophobic species including TBPB and TPPB through changes in ζ, the single decade shift in CCC for systems containing KCl may similarly involve ion adsorption. Specifically, slight preferential adsorption of K^+ ions to the negative surface of NPs may result in mild structuration.[49] Alternatively, differences in charge regulation may occur with glassy NPs exhibiting 'constant potential' behavior due to cation adsorption compared to rubbery NPs exhibiting minimal adsorption and 'constant charge' behavior, thereby yielding enhanced stability.[46] Although K^+ exhibits kosmotropic properties, slight differences in kosmotropic and chaotropic properties of monovalent ions given by the Hofmeister series has been shown to affect colloidal stability wherein chaotropic monovalent salts destabilize dispersions.[50] As a result, to ascertain differences in ion adsorption in the absence of hydrophobic interactions, PS and PI NP dispersions were salted with NH_4F, a highly kosmotropic salt, and guanidium chloride (GdmCl), a highly chaotropic salt with a delocalized positive charge. As shown in Fig. S6 (ESI†), the CCC for salted PS NP dispersions was found to vary with the Hofmeister series (GdmCl < KCl < NH_4F) while the CCC for PI NPs exhibited a different dependency (GdmCl < Nh_4F < KCl). However, comparably higher CCC's were observed for all salts in the case of PI NPs, consistent with earlier findings (Fig. 1). Therefore, while rubbery surfaces demonstrate resistance to ion adsorption, the

chaotropic and hydrophobic nature of ions is shown to strongly influence adsorption onto and the stability of glassy NPs.

Conclusions

In this study, through the fabrication of polymer NPs spanning a wide range of T_g's, we demonstrated stark differences in stability between salted dispersions of glassy and rubbery NPs. In the case of KCl which primarily alters the EDL surrounding NPs, rubbery NPs exhibited greater stability than glassy NPs as evidenced by a downward shift in CCC as polymer T_g increases above RT. For hydrophobic phosphonium cations which can directly adsorb onto NP surfaces, differences in zeta potential inversion were found, manifesting as distinct stability trends: singular instability thresholds for rubbery NPs and intermediate instability followed by re-entrant stability for glassy NPs. As a potential mechanism to rationalize the connection between T_g and ion adsorption, surface structuration as a dynamic feature of polymer NP surfaces was described, suggesting energetic limitations to ion adsorption onto the highly mobile surface layers of rubbery NPs as opposed to the relatively immobile surfaces of glassy NPs which enable adsorption according to the extended Hofmeister series.

Given these findings, future investigations to better understand impact of additional colloidal properties on the connection between T_g and NP stability are warranted. First, the impact of NP size, and therefore specific surface area ($\sim 1/r$), on stability of glassy NPs may further elucidate the proposed relation between confinement effects and interfacial ion adsorption. Second, the impact of varying NP concentration on adsorption isotherms, important for formulating dispersions for applications, can be studied. Third, the reversibility of aggregation between glassy NPs *via* transitions to rubbery could open avenues for thermo-responsive dispersions. Finally, studies connecting T_g and stability for colloids produced *via* alternate fabrication approaches such as SFEP and crosslinked colloids would expand the applicability of the observed findings.[22,51]

In applying the findings of this work, the stability of salted NP dispersions containing blends of rubbery and glassy polymers, by either mixing distinct NPs populations or generating structured Janus colloids, can also be investigated.[4,25] By judiciously selecting the concentration of hydrophobic salts, variations in surface potential of each NP population or Janus hemisphere could be partially decoupled, enabling the hierarchical assembly of oppositely-charged NPs or enhancing the wetting of net-neutral hemispheres into hydrophobic interfaces for engineering of tunable Pickering emulsifiers.

Conflicts of interest

There are no conflicts to declare.

Acknowledgements

Financial support for this work was provided by the Princeton Center for Complex Materials (PCCM), a U.S. National Science Foundation Materials Research Science and Engineering Center (Grant DMR-2011750).

References

1 K. Ulbrich, K. Holá, V. Šubr, A. Bakandritsos, J. Tuček and R. Zbořil, *Chem. Rev.*, 2016, **116**, 5338–5431.
2 R. F. Pagels and R. K. Prud'Homme, *J. Controlled Release*, 2015, **219**, 519–535.
3 A. Kirillova, C. Schliebe, G. Stoychev, A. Jakob, H. Lang and A. Synytska, *ACS Appl. Mater. Interfaces*, 2015, **7**, 21224–21225.
4 V. E. Lee, C. Sosa, R. Liu, R. K. Prud'homme and R. D. Priestley, *Langmuir*, 2017, **33**, 3444–3449.
5 B. P. Binks and S. O. Lumsdon, *Langmuir*, 2001, **17**, 4540–4547.
6 T. I. Morozova, V. E. Lee, N. Bizmark, S. S. Datta, R. K. Prud'homme, A. Nikoubashman and R. D. Priestley, *ACS Cent. Sci.*, 2020, **6**, 166–173.
7 M. E. Leunissen, C. G. Christova, A. P. Hynninen, C. P. Royall, A. I. Campbell, A. Imhof, M. Dijkstra, R. Van Roij and A. Van Blaaderen, *Nature*, 2005, **437**, 235–240.
8 In *Principles of Colloid and Surface Chemistry*, ed, P. C. Hiemenz and R. Rajagopalan, CRC Press, 3rd edn, 1997.
9 R. F. Pagels, J. Edelstein, C. Tang and R. K. Prud'homme, *Nano Lett.*, 2018, **18**, 1139–1144.
10 Y. Zhang, J. Feng, S. A. McManus, H. D. Lu, K. D. Ristroph, E. J. Cho, E. L. Dobrijevic, H. K. Chan and R. K. Prud'Homme, *Mol. Pharmaceutics*, 2017, **14**, 3480–3488.
11 S. Bhattacharjee, C. H. Ko and M. Elimelech, *Langmuir*, 1998, **14**, 3365–3375.
12 N. Eom, D. F. Parsons and V. S. J. Craig, *J. Phys. Chem. B*, 2017, **121**, 6442–6453.
13 R. F. Considine and C. J. Drummond, *Langmuir*, 2001, **17**, 7777–7783.
14 D. F. Parsons, R. B. Walsh and V. S. J. Craig, *J. Chem. Phys.*, 2014, **140**, 164701.
15 S. A. Bradford, H. Kim, C. Shen, S. Sasidharan and J. Shang, *Langmuir*, 2017, **33**, 10094–10105.
16 A. M. Smith, P. Maroni and M. Borkovec, *Phys. Chem. Chem. Phys.*, 2017, **20**, 158–164.
17 T. Cao, G. Trefalt and M. Borkovec, *Langmuir*, 2018, **34**, 14368–14377.
18 K. J. Ives, *The Scientific Basis of Flocculation*, Springer, Dordrecht, 1978, pp. 37–61.
19 C. Gauer, Z. Jia, H. Wu and M. Morbidelli, *Langmuir*, 2009, **25**, 9703–9713.
20 K. D. Ristroph, J. A. Ott, L. A. Issah, B. K. Wilson, A. Kujović, M. Armstrong, S. S. Datta and R. K. Prud'homme, *ACS Appl. Nano Mater.*, 2021, **4**, 8690–8698.
21 N. Bizmark and M. A. Ioannidis, *Langmuir*, 2015, **31**, 9282–9289.
22 L. A. Rosen and D. A. Saville, *J. Colloid Interface Sci.*, 1990, **140**, 82–92.

23 R. S. Chow and K. Takamura, *J. Colloid Interface Sci.*, 1988, **125**, 226–236.
24 L. S. Grundy, V. E. Lee, N. Li, C. Sosa, W. D. Mulhearn, R. Liu, R. A. Register, A. Nikoubashman, R. K. Prud'Homme, A. Z. Panagiotopoulos and R. D. Priestley, *ACS Nano*, 2018, **12**, 4660–4668.
25 C. Sosa, R. Liu, C. Tang, F. Qu, S. Niu, M. Z. Bazant, R. K. Prudhomme and R. D. Priestley, *Macromolecules*, 2016, **49**, 3580–3585.
26 C. Zhang, Y. Guo and R. D. Priestley, *Macromolecules*, 2011, **44**, 4001–4006.
27 Z. Fakhraai and J. A. Forrest, *Science*, 2008, **319**, 600–604.
28 D. Christie, C. Zhang, J. Fu, B. Koel and R. D. Priestley, *J. Polym. Sci., Part B: Polym. Phys.*, 2016, **54**, 1776–1783.
29 C. Zhang, Y. Guo and R. D. Priestley, *J. Polym. Sci., Part B: Polym. Phys.*, 2013, **51**, 574–586.
30 C. Zhang, V. J. Pansare, R. K. Prud'Homme and R. D. Priestley, *Soft Matter*, 2012, **8**, 86–93.
31 B. K. Johnson and R. K. Prud'homme, *AIChE J.*, 2003, **49**, 2264–2282.
32 J. Han, Z. Zhu, H. Qian, A. R. Wohl, C. J. Beaman, T. R. Hoye and C. W. Macosko, *J. Pharm. Sci.*, 2012, **101**, 4018–4023.
33 A. Nikoubashman, V. E. Lee, C. Sosa, R. K. Prud'homme, R. D. Priestley and A. Z. Panagiotopoulos, *ACS Nano*, 2016, **10**, 1425–1433.
34 X. Yan, M. Delgado, J. Aubry, O. Gribelin, A. Stocco, F. Boisson-Da Cruz, J. Bernard and F. Ganachaud, *J. Phys. Chem. Lett.*, 2018, **9**, 96–103.
35 T. I. Morozova, V. E. Lee, A. Z. Panagiotopoulos, R. K. Prud'Homme, R. D. Priestley and A. Nikoubashman, *Langmuir*, 2019, **35**, 709–717.
36 C. Calero, J. Faraudo and D. Bastos-González, *J. Am. Chem. Soc.*, 2011, **133**, 15025–15035.
37 T. Sugimoto, M. Nishiya and M. Kobayashi, *Colloid Polym. Sci.*, 2017, **295**, 2405–2411.
38 A. Martín-Molina, C. Calero, J. Faraudo, M. Quesada-Pérez, A. Travesset and R. Hidalgo-Álvarez, *Soft Matter*, 2009, **5**, 1350–1353.
39 J. Rubio and J. Goldfarb, *J. Colloid Interface Sci.*, 1971, **36**, 289–291.
40 M. W. Rutland and R. M. Pashley, *J. Colloid Interface Sci.*, 1989, **130**, 448–456.
41 J. C. J. van der Donck, G. E. J. Vaessen and H. N. Stein, *Langmuir*, 1993, **9**, 3553–3557.
42 R. Zheng, B. P. Binks and Z. Cui, *Langmuir*, 2020, **36**, 4619–4629.
43 N. Li, A. Z. Panagiotopoulos and A. Nikoubashman, *Langmuir*, 2017, **33**, 6021–6028.
44 I. Siretanu, J. P. Chapel, D. Bastos-González and C. Drummond, *J. Phys. Chem. B*, 2013, **117**, 6814–6822.
45 I. Siretanu, J. P. Chapel and C. Drummond, *ACS Nano*, 2011, **5**, 2939–2947.
46 G. Trefalt, S. H. Behrens and M. Borkovec, *Langmuir*, 2016, **32**, 380–400.
47 I. Siretanu, J. P. Chapel and C. Drummond, *Macromolecules*, 2012, **45**, 1001–1005.
48 J. R. T. Seddon and D. Lohse, *J. Phys.: Condens. Matter*, 2011, **23**, 133001.
49 I. Siretanu, H. Saadaoui, J.-P. Chapel and C. Drummond, in *Polymer Surfaces in Motion*, ed. J. Rodríguez-Hernández and C. Drummond, 2015, pp. 257–272.
50 T. Oncsik, G. Trefalt, M. Borkovec and I. Szilagyi, *Langmuir*, 2015, **31**, 3799–3807.
51 J. P. Rao and K. E. Geckeler, *Prog. Polym. Sci.*, 2011, **36**, 887–913.

